Rheological and structural properties of dilute active filament solutions

Falko Ziebert and Igor S. Aranson
Argonne National Laboratory, 9700 South Cass Avenue, Argonne, Illinois 60439, USA
(Received 16 April 2007; revised manuscript received 5 October 2007; published 24 January 2008)

The rheology and the structure of a dilute semiflexible biofilament solution, like F-actin, interacting via molecular motors is probed by molecular dynamics simulations. Oscillatory external shear is used to measure the storage and loss moduli as a function of motor activity in a range of frequencies and for low shear rates. The overall effect of the motor activity on the rheological properties is interpreted as an increase of the temperature, with the effective temperature proportional to the density of motors. However, the effect of motors on the structural properties of the solution, such as the orientation correlation function, is opposite: the motors drastically increase the orientation correlation length whereas thermal fluctuations decrease it.

DOI: 10.1103/PhysRevE.77.011918 PACS number(s): 87.16.Ka, 05.65.+b

I. INTRODUCTION

The cytoskeleton of eukaryotic cells consists of hierarchical networks of biofilaments of variable length and stiffness: from long and stiff microtubules to shorter and more flexible actin and intermediate filaments [1,2]. These networks are connected by a variety of static cross links and dynamic molecular motors. The motors generate directional forces and motion along the polar filaments through hydrolysis of adenosine triphosphate. The cytoskeletal system exhibits unique structural, transport, and rheological properties, including polar ordering of filaments, fast transport of nutrients along the networks, and nontrivial viscoelastic behavior. Molecular motors play a very important role in the organization of cytoskeletal networks and their response on external stress.

Besides obvious relevance for biology and contemporary materials science exploring "smart," self-healing materials, cytoskeletal networks attracted enormous attention in the physics community as a natural realization of an active nonequilibrium system with a multitude of interacting time and length scales. Recent experimental and theoretical studies of the cytoskeleton opened new perspectives in understanding and modeling microtubule-motor self-organization [3–10], and rheological and structural properties in actomyosin [11–14]. Significant progress was achieved in understanding the subtle rheological properties of cross-linked networks of semiflexible filaments [15–18].

In contrast, the effect of molecular motors on the rheology and structure of the cytoskeleton is still lacking proper understanding. It was suggested in Ref. [19] that the action of molecular motors in a dense suspension of filaments could be modeled by additional temperature-like fluctuations longitudinal to the filaments. The deduced high-frequency scaling has been experimentally confirmed [13], but simulation studies are missing and the behavior in the dilute case, where this kind of statistical description no longer applies, is still unexplored. The lack of simulation results is not surprising: the problem involves many vastly different time scales which must be resolved by the algorithm, fast scales associated with the diffusion of motors in the bulk and to the motion of motors on filaments, and the very slow time scale of the overall structure evolution. As a result, only relatively small systems have been studied so far [3,4], and the long-term behavior as well as the rheology have not been addressed.

Here we have performed molecular dynamics simulations of two-dimensional solutions of semiflexible polar filaments interacting via molecular motors. Thanks to an algorithm allowing one to exclude the short time scale associated with motor diffusion, we were able to simulate rather large systems of actin-like filaments interacting with a large number of motors on macroscopically large time intervals (hours). We monitored the response on external oscillatory shear stress and observed the orientation correlation function over a large time interval. We found that the motor-related contribution to the viscoelastic properties such as storage (or elastic) and loss moduli can be indeed described by an increase of a certain effective temperature monotonously increasing with motor density or attachment rate. However, this description appears to be incomplete and does not adequately address the corresponding change in the structure. In contrast, the orientation correlation length characterizing polar ordering of the filaments shows an opposite trend: it increases with increasing motor density but decreases with the increase of thermodynamic temperature.

II. METHOD

We focus on two-dimensional solutions of N semiflexible polar filaments of identical length L. For the sake of simplicity hydrodynamic interactions are not included. Also, excluded volume and entanglement effects are considered to be negligible in a quasi-two-dimensional situation as in most of the experiments. Accordingly the filaments interact only through the motors.

A. Simulation technique for semiflexible filaments

The filaments are represented by space curves $\mathbf{r}(s)$ parametrized by their arclength s. The equation of motion of an individual filament follows from the balance between viscous drag $\zeta\dot{\mathbf{r}}$, bending force $\mathbf{F}_b$, filament tension $\mathbf{F}_t$, stochastic force due to thermal fluctuations $\mathbf{F}_n$, external force $\mathbf{F}_s$, and motor force $\mathbf{F}_m$, only the latter giving rise to filament-filament interactions,

$$\zeta\dot{\mathbf{r}} = \mathbf{F}_b + \mathbf{F}_t + \mathbf{F}_n + \mathbf{F}_s + \mathbf{F}_m. \quad (1)$$

The bending force for semiflexible filaments is of the form $\mathbf{F}_b = -\beta\partial_s^4\mathbf{r}(s)$, with a bending stiffness of $\beta = 0.073$ pN μm^2 for actin [20]. To evaluate the tension force, we discretized the filament with a step size d_0 along the arclength and imposed stiff springs between nearest-neighbor sites, $\mathbf{F}_t = -\nabla V(r)$, with the interaction potential $V(r) = a(r-d_0)^2$ and sufficiently large a (we use $a=10$ which ensures that filament extension is in the 0.1% range). As filament length we used $L=20$ μm and as discretization length $d_0 = 0.5$ μm, being several times smaller than the thermal persistence length. The friction coefficient per length is $\zeta = 6\pi\eta d_0$ with η the solvent viscosity (chosen as 10 times the one for water). Finally, for the random force due to thermal fluctuations, $\mathbf{F}_n$, we use isotropic δ-correlated noise with a strength $\langle \mathbf{F}_n(\mathbf{r},t)\mathbf{F}_n(\mathbf{r}',t')\rangle = S^2\delta(\mathbf{r}-\mathbf{r}')\delta(t-t')$. To introduce an oscillatory shear force in the x direction with frequency ω and amplitude κ, a term $\mathbf{F}_s = \kappa\mathbf{x}_0 \sin(\omega t)y$ was added, with $\mathbf{x}_0$ being the unit vector along the x direction. The resulting system of $2\times N$ partial differential equations was solved by the Crank-Nicholson implicit technique.

B. Implementation of molecular motors

The motors are modeled by short stiff springs connecting the two "head" regions attached to the filaments. As mentioned above, one of the short (but irrelevant) time scales in the problem is associated with motor diffusion in the solution. In order to bypass this computational bottleneck, we applied the following algorithm: instead of following motor trajectories in solution, we track the intersections between different filaments and introduce motors at the intersection points with a certain attachment rate m_a. Assuming that the motors are rather homogenized by the fast diffusion, the attachment rate m_a should be proportional to the mean motor density. Accordingly, this algorithm corresponds to the situation when motors are abundant in the system which is characteristic for many experiments (e.g., those in [12]). After attaching to an intersecting pair of filaments, the motor heads start to walk with a velocity v (usually chosen as 1 μm/s) along both filaments and acting like a moving linear spring between the two attachment points $\mathbf{r}_1, \mathbf{r}_2$ with spring constant K [4]. After each step the motor may detach with a second probability m_d, as well as if the motor reaches a filament end or if the motor force $\mathbf{F}_m = \pm K(\mathbf{r}_1 - \mathbf{r}_2)$ exceeds a certain threshold $\mathbf{F}_{\max}$. For simplicity we did not implement a nontrivial force-velocity relation. We also neglected multiple intersections of the same two filaments, which is a rare event and should be not important. However, our algorithm takes into account the action of many motors per filament due to intersections with many filaments. We also verified that the two-filament behavior is consistent with the results of Ref. [21].

C. Evaluation of stresses and strains

The total stress σ_{ij} is evaluated by the Kirkwood formula [22] $\sigma_{ij} = \langle P^{-1}\Sigma(\mathbf{r}_i - \mathbf{r}_i^0)\mathbf{F}_j\rangle$, where $\mathbf{r}^0$ is the center of mass of a single filament, $\mathbf{r}$ is the position of the discretization node on the filament, $\mathbf{F}$ is the sum of all forces acting on that node, and P is the number of nodes per filament (we usually simulated $N=1000$ filaments, with $P=40$ nodes each). The stress due to thermal fluctuations is evaluated by the method introduced in Ref. [23]. To calculate the strain we divided the simulation domain along the x direction in several layers and determined the displacement of the centers of mass of each layer.

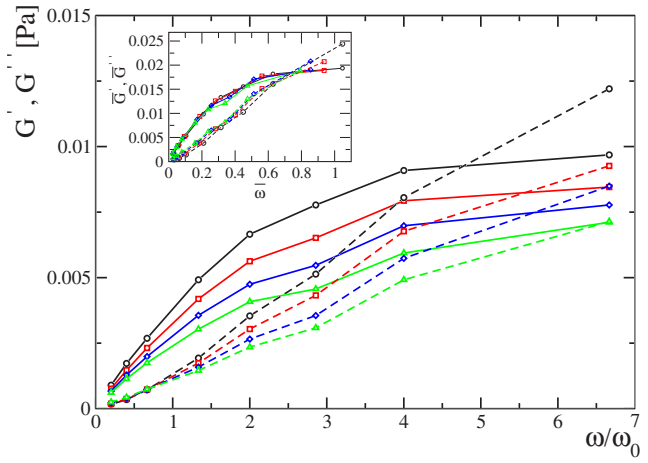

FIG. 1. (Color online) The elastic, G' (dashed lines), and loss, G'' (solid lines), moduli as a function of the external driving frequency ω in units of ω_0 in the absence of motors and for different amplitudes of noise, $S=0.04$ (○), 0.05 (□), 0.06 (◇), 0.07 (△), corresponding to temperatures $T \simeq 308$, 481, 692, 942 K, respectively. Inset: G' and G'' collapsed by the scaling $\bar{G} = \sqrt{S}G$, $\bar{\omega} = \omega/\sqrt{S}$.

III. RESULTS

A. Scaling behaviors for storage and loss moduli

First we evaluated the storage and loss moduli, $G'(\omega)$ and $G''(\omega)$, in the absence of motors, i.e., for noninteracting filaments. Simulations were performed in the range of temperatures (noise amplitudes) and frequencies of oscillatory shear ω as shown in Fig. 1. For dilute solutions of semiflexible filaments three different regimes have been established [24,25]: for very low frequencies, $\omega < \tau_\perp^{-1} = \left(\frac{\zeta L^4}{k_B T L_p}\right)^{-1}$ with $L_p = \frac{\beta}{k_B T}$ the persistence length, the behavior is that of rigid rods [22], $G \propto k_B T i\omega\left(\frac{3}{4}\frac{1}{1+i\omega\tau_r} + \frac{1}{4}\right)$, governed by rotational diffusion with characteristic time $\tau_r = 1/6D_r$. For high frequencies, $\omega \gg \tau_\parallel^{-1} = \left(\frac{\zeta L^8}{k_B T L_p^5}\right)^{-1}$, the modulus scales like $\frac{1}{k_B T}\omega^{3/4}$. For $L < L_p$, a third regime with a $\omega^{5/4}$ scaling has been found [25], which, however, does not apply to our case where $L \simeq L_p$.

Since we are finally interested in the effects of motors on the system and the time scale of motor motion is about the filament length divided by the motor velocity, evaluating to several seconds and $\omega_0 = 2\pi\frac{v}{L} \simeq 0.31$, we have chosen an intermediate frequency regime, which is also suggested by recent experiments [14]. In this intermediate frequency range

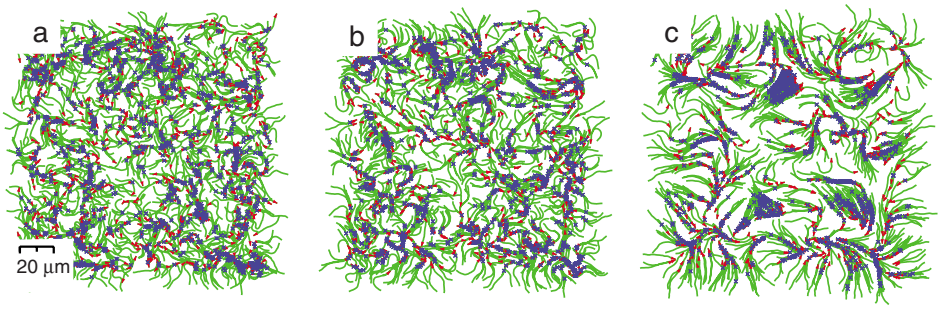

FIG. 2. (Color online) Simulation snapshots at times (a) $t=50$ s, (b) $t=200$ s, (c) $t=2000$ s for a motor attachment rate of $m_a=0.5$ s^{-1}. The filaments are shown as solid lines (green) with the arrowheads displaying the filament polarity (i.e., the direction of motion of the motors along the filaments). The crosses (blue) are the positions of the motor "head" regions. Simulations were performed for $N=1000$ filaments of length $L=20$ μm. For this attachment rate, the average number of motors is about 1200.

where one expects effects of the motors, there is not a defined scaling. Therefore, we collapse both $G'(\omega)$ and $G''(\omega)$ simultaneously, which is done best by the empirical scaling $G\to\bar{G}=G\cdot\sqrt{S}$ and $\omega\to\bar{\omega}=\omega/\sqrt{S}$ with S the noise strength, as shown in the inset of Fig. 1. The observed empiric scaling of the moduli G with temperature is thus roughly $G\sim 1/\sqrt{T}$, intermediate between the low- and high-frequency behavior.

Now let us turn to the effects of motors. Figure 2 exemplifies the temporal evolution of a filament-motor system with a high motor attachment rate of $m_a=0.5$ s^{-1}. As an initial condition we used a well-thermalized isotropic solution of noninteracting filaments. After a short time interval, the filament ends (marked by red arrowheads) start to align, leading to an intermediate polarity sorting phenomenon (see below). At later stages, polar bundling of filaments and void formation ensues. Additionally, filaments initially oriented outwards to the boundary of the filament drop are redirected or drawn inside the drop.

The motors have a profound effect on the rheology, see Fig. 3. Both moduli $G'(\omega)$ and $G''(\omega)$ decrease substantially with the increase of motor activity, i.e., the motors make the system more fluidized, qualitatively similar to heating and the behavior reported in [11]. The presence of motors, which drive the system out of equilibrium, can be captured on the phenomenological level by introducing an effective or active temperature T_a as compared to the thermodynamic temperature T_{th}. To quantify this effect, we again performed a collapse of both moduli simultaneously. By comparing with the equilibrium result in the absence of motors, Fig. 1, we deduced the effective temperature T_a as a function of the average number of attached motors, as shown in Fig. 4. As compared to the value of thermodynamic temperature, chosen as $T_{\text{th}}=308$ K, the motor activity gives rise to an effective temperature of up to 3000 K, where the effect of motors seems to saturate. Thus, the concept of an *isotropic* effective temperature captures correctly the trend in the rheology in the presence of motors.

We should mention that the accessible frequency range is restricted for two reasons: In the presence of motors, for very low frequencies ω, measurements become ambiguous since the system does not reach a stationary state for quite a long time due to polar ordering, cf. the growth of the correlation length in Fig. 5. Oppositely, for high frequencies we obtained an (artificial) peak in the loss modulus associated to the finite extensibility of filaments. Due to numerical algorithm limitations we had to take the value of a in $\mathbf{F}_t$ significantly lower than the realistic value for actin filaments [26]. Thus, in order to obtain the high-frequency scaling, a more sophisticated algorithm concerning the filament dynamics and also a more elegant way of the stress evaluation should be used, cf. [21,25].

B. Estimate for the effective temperature

The effect of the motors can be estimated as follows. The additional energy E_t injected in the system by the motors moving on more than one filament simultaneously is roughly $E_t\approx\langle|F|\rangle\langle l\rangle M/N$, where $\langle|F|\rangle$ is the typical motor force acting on the filaments, $\langle l\rangle$ is the run length of the motors, and M/N is the average number of motors per filament. Note that

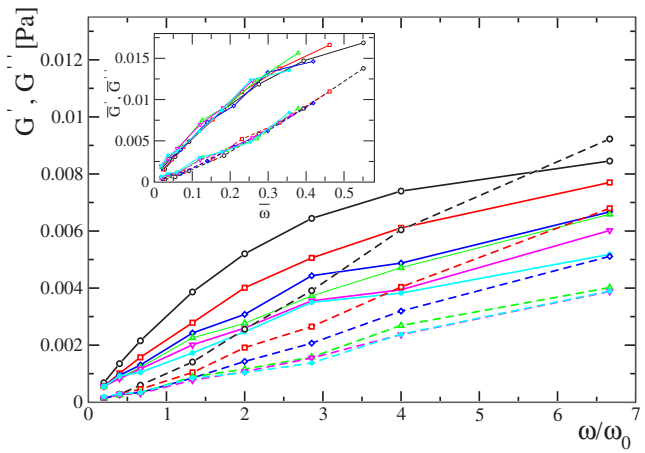

FIG. 3. (Color online) The elastic, G' (dashed lines), and loss, G'' (solid lines), moduli as a function of the external driving frequency ω in units of the characteristic motor frequency ω_0 for different values of the motor attachment rate: $m_a=0.01$ (○), 0.03 (□), 0.06 (◇), 0.1 (△), 0.2 (▽), 0.5 (●), and fixed detachment rate $m_d=0.1$ s^{-1}. Inset: Data collapse used to extract an active temperature.

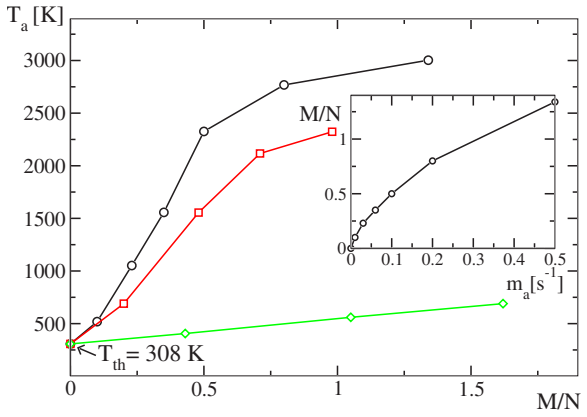

FIG. 4. (Color online) Active temperature T_a (K) vs average number of motors per filament, M/N, as extracted from the data as shown in Fig. 3. Motor velocity $v=1$ μm/s (○), $v=0.5$ μm/s (□), $v=0.1$ μm/s (◇). Thermodynamic temperature $T_{\mathrm{th}}=308$ K. Inset: M/N as a function of motor attachment rate m_a for the case $v=1$ μm/s and for fixed detachment rate $m_d=0.1/\mathrm{s}^{-1}$.

motors attached only to one filament are not considered in our algorithm. If one considers the filaments as infinitely long, the run length $\langle l\rangle$ is determined by the typical motor velocity V and the detachment probability m_d, $\langle l\rangle \approx V/m_d$. However, one must account for the fact that the filaments are finite and that motors attach at the intersection point. If one assumes that the intersection points are distributed with equal probability, for a filament length of 20 μm and $m_d=0.1$ s^{-1}, one obtains $\langle l\rangle \approx 5$ μm. This value holds only for the simplest case of nearly parallel filaments, while for larger angles the motor detaches much earlier due to the detachment upon reaching a maximum force. So the run length can be estimated as 1–3 μm. Since the motors move with constant velocity for not too high load, the typical force is in leading order $\langle |F|\rangle \approx V\langle |\sin(\phi)|\rangle$, where ϕ is the local angle between the filaments at the intersection point. For large angles ϕ the run length becomes very small. Moreover, the intersection point moves along with the attached motor, so 0.1 pN is a reasonable value for the typical force. In total, we estimate $k_BT_a=E_t\approx 0.1$ pN$\times 1$ μm$\times M/N$, which for high attachment rates ($M/N\simeq 1$) leads to $T_a\simeq 7000$ K, in reasonable agreement with our simulation results. The saturation of the active temperature for high attachment rates is most probably due to the reorganization of the filaments in parallel bundles, where there is not much displacement of filaments anymore. From the above estimate it is also clear that a smaller motor velocity leads to smaller active temperature, since both the typical force and the run length decrease. Also, increasing the detachment rate naturally leads to a decrease in the active temperature. Both dependencies were checked with select simulation runs; the dependence on the motor speed is shown in Fig. 4.

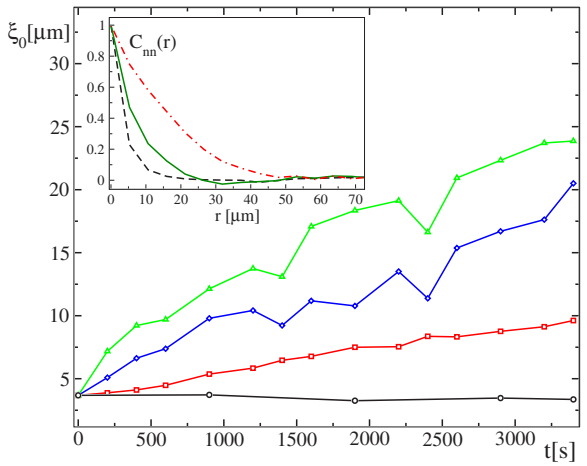

FIG. 5. (Color online) The correlation length ξ_0 vs time without motors (○), and with motors, attachment rates $m_a=0.01$ (□), 0.1 (◇), 0.5 (△). Inset: The correlation function $C_{nn}(r)$ without motors (dashed line), with motors at $t=200$ (solid line), and at late time $t=2000$ (dashed-dotted line).

C. Evolution of structural properties

To obtain insights into structural properties, like polar ordering, we calculated the correlation function of the filament orientation, $C_{nn}(\mathbf{r}-\mathbf{r}')=\langle \mathbf{n}(\mathbf{r})\mathbf{n}(\mathbf{r}')\rangle$, where $\mathbf{n}(\mathbf{r})$ is the local filament orientation unit vector. From this function we calculated the radial correlation length ξ_0 by a fit to an exponential decay. The temporal evolution of the correlation length is shown in Fig. 5. In the absence of motors it is small (in the order of the thermal persistence length) and does not change in time. While for low motor activity the growth is rather linear, high motor activity induces a growth of ξ_0 with time roughly like $\sqrt{t}$ due to the profound bundling and straightening (or zipping, cf. [28]) of the filaments. The square-root behavior can be anticipated for the two-dimensional aggregation phenomenon constrained by total mass conservation. The inset to Fig. 5 shows the temporal evolution of the correlation function: at intermediate times (solid line) there is a small dip around double the filament length associated likely with the effect of polarity sorting, meaning that motors are separating filaments with opposite orientations [27]. At later times (dashed-dotted line) the correlation length increases substantially and, for high attachment rates, it becomes even larger than the filament length. The polar ordering of the filaments obviously cannot be described by the concept of effective temperature: A temperature increase leads to the opposite effect, i.e., *decreases* the correlation length.

IV. CONCLUSIONS

We have performed Langevin-type simulations of semiflexible filaments, such as actin, interacting through molecular motors. We investigated the rheology and, due to an algorithm that allows us to study the long time behavior by circumventing motor diffusion, also the structural properties. The phenomenological concept of an effective temperature

appears to describe reasonably well the rheology of dilute active filament-motor systems if, as in our case, the contribution to the total stress due to polar ordering effects is relatively small. The obtained dependence of the active temperature on the motor activity, Fig. 4, is of value for continuum treatments of these systems and agrees reasonably with ongoing experiments [29]. The concept of effective temperature fails, however, to address the structural properties of polar organization for large time scales. In contrast to entangled systems [13,19], where the active temperature is assumed to be anisotropic and the correlation length decreases with motor activity, here, in the dilute case, the active temperature is isotropic and the correlation length increases due to filament bundling.

Thus, our results provide nontrivial insight into the evolution of complex active systems such as the cytoskeleton, and our algorithm opens perspectives in modeling and design of theoretical concepts for active filaments networks. There are many possible extensions of our work, one of the most intriguing questions being the simultaneous action of motors and static cross links. Simulations of cross-linked filaments (without motors) show that the moduli increase quite rapidly with increasing number of cross links, as expected. Three-dimensional simulations of cross-linked filaments were also recently reported in [31]. Together with motors, bundled structures reminiscent of those obtained by experiments and continuum theories can be obtained [12,30].

ACKNOWLEDGMENTS

The authors thank Joseph Käs, Lev Tsimring, Walter Zimmermann, Francois Nédélec, Gijsje Koenderink, and David Weitz for useful discussions. This work was supported by the U.S. DOE Grant No. DE-AC02-06CH11357.

[1] H. Lodish, A. Berk, S. L. Zipursky, P. Matsudaira, D. Baltimore, and J. Darnell, *Molecular Cell Biology* (Freeman, New York, 1999).
[2] A. Bausch and K. Kroy, Nat. Phys. **2**, 231 (2006).
[3] F. J. Nédélec, T. Surrey, A. C. Maggs, and S. Leibler, Nature (London) **389**, 305 (1997).
[4] F. J. Nédélec, J. Cell Biol. **158**, 1005 (2002).
[5] T. Surrey, F. Nédélec, S. Leibler, and E. Karsenti, Science **292**, 1167 (2001).
[6] T. B. Liverpool and M. C. Marchetti, Phys. Rev. Lett. **90**, 138102 (2003).
[7] K. Kruse, J. F. Joanny, F. Jülicher, J. Prost, and K. Sekimoto, Phys. Rev. Lett. **92**, 078101 (2004).
[8] I. S. Aranson and L. S. Tsimring, Phys. Rev. E **74**, 031915 (2006).
[9] F. Ziebert and W. Zimmermann, Eur. Phys. J. E **18**, 41 (2005).
[10] P. Kraikivski, R. Lipowsky, and J. Kierfeld, Phys. Rev. Lett. **96**, 258103 (2006).
[11] D. Humphrey, C. Duggan, D. Saha, D. Smith, and J. Käs, Nature (London) **416**, 413 (2002).
[12] D. M. Smith, F. Ziebert, D. Humphrey, C. Duggan, M. Steinbeck, W. Zimmermann, and J. Käs, Biophys. J. **93**, 4445 (2007).
[13] L. LeGoff, F. Amblard, and E. M. Furst, Phys. Rev. Lett. **88**, 018101 (2001).
[14] D. Mizuno, C. Tardin, C. F. Schmidt, and F. C. MacKintosh, Science **315**, 370 (2007).
[15] J. Wilhelm and E. Frey, Phys. Rev. Lett. **91**, 108103 (2003).
[16] D. A. Head, A. J. Levine, and F. C. MacKintosh, Phys. Rev. Lett. **91**, 108102 (2003).
[17] C. Storm, J. J. Pastore, F. C. MacKintosh, T. C. Lubensky, and P. A. Janmey, Nature (London) **435**, 191 (2005).
[18] C. Heussinger and E. Frey, Phys. Rev. Lett. **97**, 105501 (2006).
[19] T. B. Liverpool, A. C. Maggs, and A. Ajdari, Phys. Rev. Lett. **86**, 4171 (2001).
[20] F. Gittes, B. Mickey, J. Nettleton, and J. Howard, J. Cell Biol. **120**, 923 (1993).
[21] D. Karpeev, I. S. Aranson, L. S. Tsimring, and H. G. Kaper, Phys. Rev. E **76**, 051905 (2007).
[22] M. Doi and S. F. Edwards, *The Theory of Polymer Dynamics* (Clarendon, Oxford, 1986).
[23] P. S. Doyle, E. S. G. Shaqfeh, and A. P. Gast, J. Fluid Mech. **334**, 251 (1997).
[24] F. Gittes and F. C. MacKintosh, Phys. Rev. E **58**, R1241 (1998).
[25] M. Pasquali, V. Shankar, and D. C. Morse, Phys. Rev. E **64**, 020802(R) (2001).
[26] X. Liu and G. H. Pollack, Biophys. J. **83**, 2705 (2002).
[27] A. B. Verkhovsky, T. M. Svitkina, and G. G. Borisy, J. Cell Sci. **110**, 1693 (1997).
[28] J. Uhde, M. Keller, E. Sackmann, A. Parmeggiani, and E. Frey, Phys. Rev. Lett. **93**, 268101 (2004).
[29] D. A. Weitz (private communication).
[30] F. Ziebert, I. S. Aranson, and L. S. Tsimring, New J. Phys. **9**, 421 (2007).
[31] E. M. Huisman, T. van Dillen, P. R. Onck, and E. Van der Giessen, Phys. Rev. Lett. **99**, 208103 (2007).